Quantum optics lab report

Jacopo Tissino

2020-05-30

Abstract

We present the results of two experiments in quantum optics. The first is a repetition of the one originally performed by Grangier, Roger, and Aspect [GRA86], which shows that light is made up of indivisible quanta. The second one provides and tests a convenient low-tech way to turn a coherent LASER state into a thermal state.

1 Indivisibility of the photon

1.1 Background

The fact that light is made up of indivisible photons is not the only possible explanation for the photoelectric effect [Tho+04]: it can also be described with a quantized surface and a classical electromagnetic field.

So, we need an experiment to unambiguously show that light is indeed made up of indivisible *quanta*.
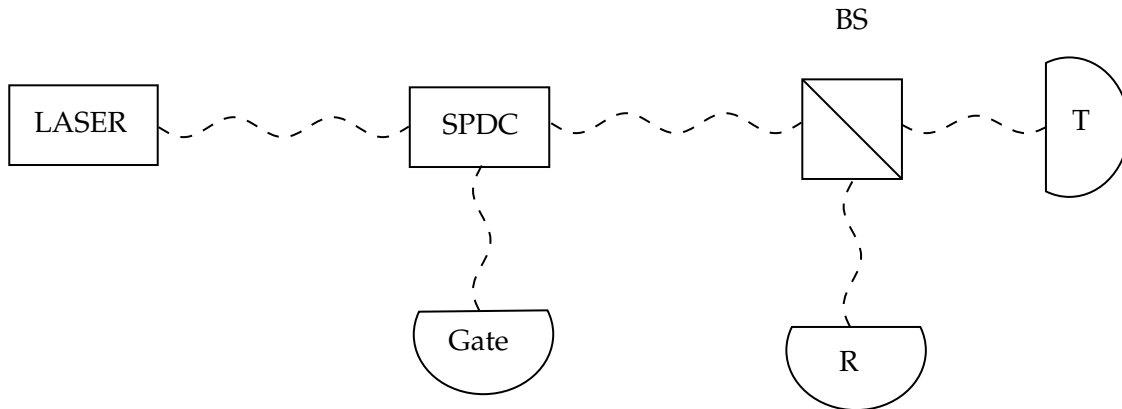
1.2 Experimental setup

Figure 1: Indivisibility experiment setup.

A schematic for the apparatus is provided in figure 1. A LASER produces a coherent beam of light, whose photons have energy $2\hbar\omega$. This beam impacts upon a nonlinear crystal,

where a photon each $10^6 \div 10^8$ undergoes Spontaneous Parametric Down-Conversion, being split into two entangled photons, each with energy $\hbar\omega$. These are emitted in two cones which intersect along two rays.

Along one of these the photon is sent to a detector called "Gate", along the other the photon is sent towards a beamsplitter; from this it can go to either of two detectors, which are called "T" and "R" for "Transmitted" and "Reflected".

Each detector has a nonzero "dark count" — clicks in the absence of a photon —, and an efficiency different from 100%. Also, photons might be absorbed by the air in their path or by the beamsplitter.

Let us first consider the problem ideally, in the absence of these sources of error. Then, a click in the "Gate" detector signals that a photon is also coming through the beamsplitter.

Then, according to quantum theory if that photon is reflected it is not transmitted, and vice versa. If, instead, we describe the electromagnetic field classically we expect the detection probability per unit time for both "R" and "T" to be proportional to the incoming power, with no correlation nor anticorrelation between them.

We may quantify this by introducing the second order time coherence parameter

$$g^{(2)}(0) = \frac{\mathbb{P}(RT|G)}{\mathbb{P}(R|G)\mathbb{P}(T|G)}, \tag{1}$$

where by $RT|G$ we mean the event of observing a R+T coincidence, conditioned upon seeing a click by the gate; the notation for the other ones is similar. We will omit the argument (0) hereafter; different values for it would indicate measurement of correlations at different times.

This can be computed by counting the number of coincidences, the expression is

$$g^{(2)}_{\text{measured}} = \frac{N_{TRG}N_G}{N_{RG}N_{TG}}. \tag{2}$$

This parameter allows us to quantify the correlation or anticorrelation between the detectors: let us consider some simple cases.

1. In quantum theory, we expect $\mathbb{P}(RT|G) = 0$, since the photon cannot be detected at both sides — therefore $g^{(2)} = 0$.

2. In classical theory, we expect $\mathbb{P}(RT|G) = \mathbb{P}(R|G)\mathbb{P}(T|G)$, since the events are independent, at each moment in time. If the laser's intensity is constant this can be extrapolated through the whole observation to yield $g^{(2)} = 1$.

3. In classical theory we can also consider the effect of a time-varying intensity. In that case, this intensity $I(t)$ is split into $\mathcal{T}I(t)$ and $\mathcal{R}I(t)$ at the beamsplitter, where $\mathcal{T}$ and $\mathcal{R}$ are the transmission and reflection coefficients, satisfying $\mathcal{T} + \mathcal{R} = 1$. Then, we get

$$g^{(2)} = \frac{\int \mathcal{T}I(t)\mathcal{R}I(t)\,\mathrm{d}t}{\int \mathcal{T}I(t)\,\mathrm{d}t \int \mathcal{R}I(t)\,\mathrm{d}t} \geq 1, \tag{3}$$

by the Cauchy-Schwarz inequality. All the temporal integrals are definite ones, the bounds corresponding to the time of observation. For a small enough temporal variation of the intensity, the result approaches 1.

This is all in the case of an ideal detector, with no losses nor dark count. We do not explore the effect of these sources of error theoretically; instead, in the data analysis they are parametrized and simulated as stochastic variables.

1.3 Data preparation

The output of the timetagger is a table of times and corresponding channel values. Each entry of this table represents a photon detection at a single detector. The times are expressed as integer multiples of the temporal resolution of the timetagger, which is nominally 80.955 ps.

There is a complication: the timetagger exhibits a slight preference for odd values of the integer which represents the time, as opposed to even ones. This effect does not pose an issue for our analysis, as long as we bin our arrival times in time intervals of 2×80.955 ps.

We want to calculate **coincidences**. The temporal resolution we have corresponds to a length scale of around 5 cm, which is smaller than the size of the apparatus, so we are able to see systematic time differences between the arrival times corresponding to the light's travel time.

In figure 2 we plot the differences between the arrival times of photons to either R or T and the gate.
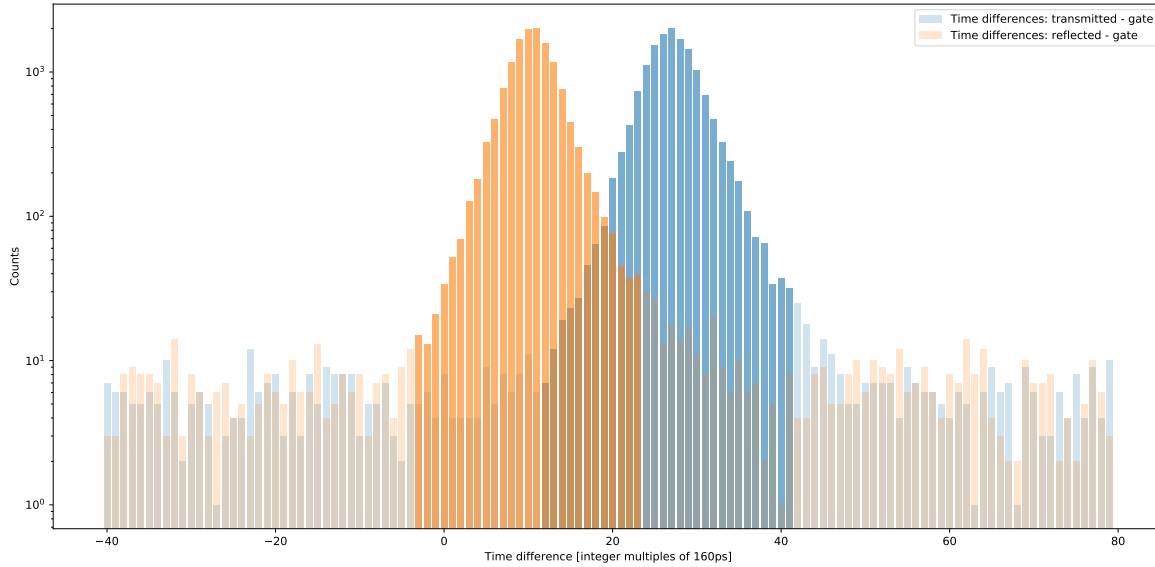

Figure 2: Time differences. In a darker colour the events which were counted as coincidences are shown.

We see distinct Gaussian peaks a few nanoseconds away from zero. We fit these, and find the means to be 10 and 27 respectively, while the standard deviations are both around 3.

Outside of these peaks, there is a constant noise background of the order of 10 detections per Δt bin. We choose to consider as coincidences events which lie within 5 standard

deviations in each peak, since around that point the values become compatible with those of the background.

This allows us to compute N_{RG} and N_{TG}; N_G is simply the total count of the gate; for N_{TRG} we count a coincidence if we have a coincidence on both R and T corresponding to the *same* gate tick.

This procedure yields $N_G = 1554341$, $N_{TG} = 14829$, $N_{RG} = 13870$, $N_{TRG} = 2$. Therefore, we compute the preliminary result:

$$g^{(2)} \approx 0.015 \,. \tag{4}$$

1.4 Simulation

In order to perform a proper Bayesian analysis of these results, we need to compute the Bayes Factor in:

$$\frac{\mathbb{P}(\text{quantum}|\text{data})}{\mathbb{P}(\text{classical}|\text{data})} = \underbrace{\frac{\mathbb{P}(\text{data}|\text{quantum})}{\mathbb{P}(\text{data}|\text{classical})}}_{\text{Bayes Factor}} \frac{\mathbb{P}(\text{quantum})}{\mathbb{P}(\text{classical})} \,. \tag{5}$$

Some clarifications are in order. By "data" we mean the tuple $(N_G, N_{TG}, N_{RG}, N_{TRG})$. I use the notation $\mathbb{P}$ for ease of reading, but the Bayes Factor is really a ratio of two probability *densities*.[1] The two models — quantum and classical — are simulated and an estimate for the *BF* is calculated as follows.

1. The number N_G is fixed as the total number of potential event detections for either detector.

2. We set two parameters: r, the detection rate, and e, the error rate. Each detector is assumed to detect a fraction r of the incoming photons, and to make an error a fraction e of the time — this can be either a dark count, or a missed detection (although since $r \ll 1$, it mostly accounts for the former).[2]

3. In the classical case, the detectors are simulated independently, while in the quantum case a "which-way" parameter is simulated with a $1/2$ chance for either direction, and only the selected detector may see the photon. In order to account for the halving of the number of photons seen globally (and to compare the numbers for the classical and quantum case directly), the detection rate for the classical case is halved.

4. The computation for $\mathbb{P}(\text{data}|M)$ where M is a model is as follows:

$$\mathbb{P}(\text{data}|M) = \int \mathbb{P}(\text{data}|M; r, e) f(r) f(e) \, dr \, de \,, \tag{6}$$

---

[1] Or rather, since the detection numbers are so large, it is convenient to model them as continuous.

[2] A small correction is needed to account for the detector asymmetry. We observe $N_{TG} - N_{RG} \approx 1000$, which is on the order of 8σ using Poisson statistics ($\sqrt{N_{TG}} \approx 122$): so, there is a bias in the detectors or in the beamsplitter — we cannot tell, but surely it is the case that statistically more coincidences are detected in one detector than the other. This is accounted for by calculating the factor $b = N_{TG}/N_{RG}$ from the data and applying it as a *constant bias* for each simulated ratio between the detectors, for both models. So, if one detector is simulated to have a rate r the other one is simulated to have a detection rate br.

where $f(r)$ and $f(e)$ are the prior probability distributions for the detection rate and the error rate. Both of these are chosen to be uniform, and their ranges are not constrained *a priori* to be smaller than $[0, 1]$; however after exploratory runs it was found that the likelihoods for both models were nonzero only in a certain region, so only those were simulated for computational efficiency.

The definitive intervals are $r \in [0.012, 0.019]$ and $e \in [3.0 \times 10^{-7}, 1.8 \times 10^{-2}]$; 50 points are simulated for each, they are linearly spaced for r and logarithmically spaced for e.

5. For each pair of parameters, N_G photons are simulated for N_{sim} times. In the final run, we set N_{sim} to 600.

   For each of the N_{sim} simulations the values N_{TG}, N_{RG} and N_{TRG} are extracted (also, trivially, the fixed value of N_G). From these, a gaussian Kernel-Density Estimation technique (using Scott's rule [con19; Sco15]) is used to estimate the value of the multivariate PDF at the point corresponding to the measured data for both models: the likelihood of the data. The variation of these likelihoods is shown in figure 3.

6. These likelihoods are integrated along r and e to yield a total value. We find

$$BF = \frac{\mathbb{P}(\text{data}|\text{quantum})}{\mathbb{P}(\text{data}|\text{classical})} \approx 10^{77} . \tag{7}$$
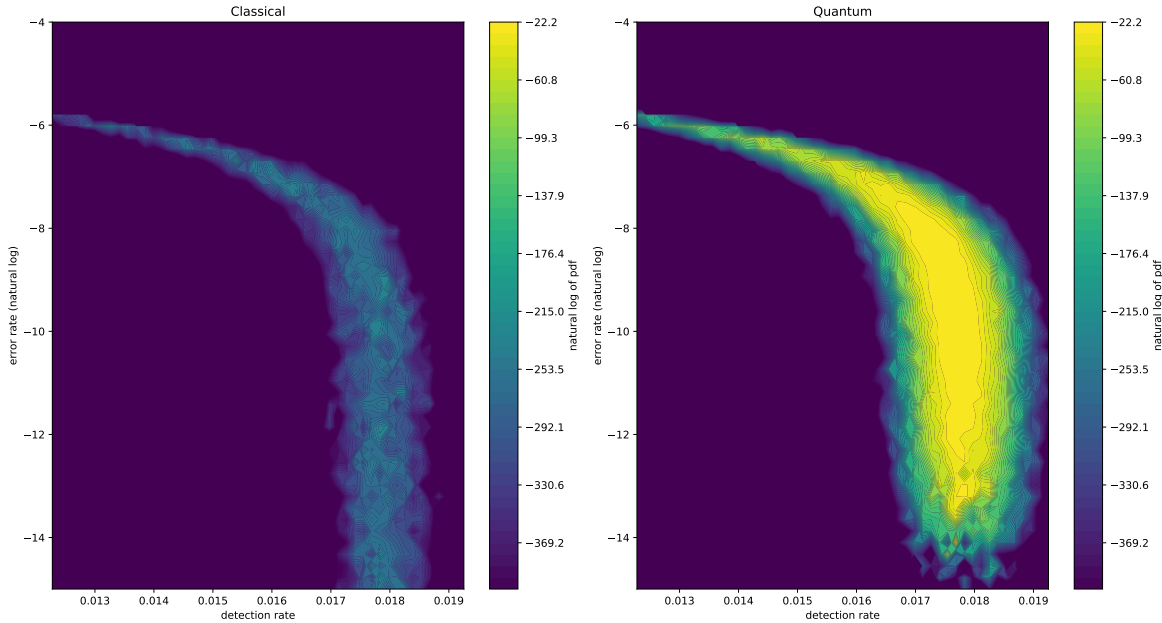

Figure 3: Log-PDFs for the classical and quantum cases. Note the log-scale of the colours: the likelihood of the classical model is *heavily* suppressed compared to the one of the quantum model.

The code which performs these simulations can be found at https://github.com/jacopok/quantum_optics/tree/master/single_photon.

5

A note on the parametrization: we use only two parameters for our model because it is the least amount which can reproduce the experimental results. This is certainly a heavy simplifying assumption: we are considering each gate click as "guaranteed", and putting all the uncertainty in the other two detectors. This may seem like an issue, but it is not. The effect of errors (dark count and missed photons) in the gate and in the detectors is always a bit-flip in the end, so we can parametrize away our ignorance of the precise cause of a certain error.

Since we have to marginalize over any new parameter we introduce, we are forced to have a small number of them to have a computationally tractable problem.

The final result is extremely favorable towards the quantum theory of light.

2 Photon statistics

2.1 Background

Just like the classical Maxwell equations take the form of a classical harmonic oscillator, a single mode of the photon field can be described as a quantum harmonic oscillator.

We wish to describe photon statistics pertaining to a laser beam, so we are justified in fixing the ω of the light.

Coherent light is the closest quantum approximation we can find for the monochromatic plane wave solution. A coherent state $|\alpha\rangle$ can be defined to be an eigenstate of the annihilation operator $\hat{a}$: $\hat{a}|\alpha\rangle = \alpha|\alpha\rangle$.

We can write these states in terms of the Fock number states $|n\rangle$ as:

$$|\alpha\rangle = \exp\left(-\frac{|\alpha|^2}{2}\right) \sum_n \frac{\alpha^n}{n!} |n\rangle \, , \tag{8}$$

and the expectation value of the electric field in a certain direction is oscillatory as expected:

$$\langle\alpha|\hat{E}_x|\alpha\rangle = i\sqrt{\frac{\hbar\omega}{2\epsilon_0 V}}\left(\alpha e^{ik_\mu x^\mu} - \alpha^* e^{-ik_\mu x^\mu}\right) , \tag{9}$$

where we use the mostly plus metric convention, ϵ_0 is the vacuum dielectric permittivity and V is the volume of the "box" in which the field is contained. The average number of photons is given by $\bar{n} = |\alpha|^2$, and with this we can describe the statistics of the number of photons we would find in a certain region: it follows a Poisson distribution,

$$\left|\langle\alpha|n\rangle\right|^2 = \frac{e^{-\bar{n}}\bar{n}^n}{n!} \, . \tag{10}$$

Thermal light, on the other hand, has the distribution we would expect to see if, for instance, we had a bath of atoms in thermal equilibrium with radiation and a transition with energy $\hbar\omega$ [ST, section 14.4].

The distribution describing this situation is the Boltzmann one:

$$\mathbb{P}(E_n) \propto \exp\left(-\frac{E_n}{k_B T}\right) , \tag{11}$$

and in our case, using $E_n = n\hbar\omega$ and the fact that the mean photon number is given by

$$\bar{n} = \frac{1}{\exp(\hbar\omega/k_B T) - 1},\tag{12}$$

we can write this as

$$\mathbb{P}(n) = \frac{1}{\bar{n}+1}\left(\frac{\bar{n}}{\bar{n}+1}\right)^n.\tag{13}$$

In quantum terms, this is a *completely mixed* state, a classical probabilistic mixture of the number states $|n\rangle$, described by the density matrix

$$\rho_{\text{thermal}} = \sum_n \mathbb{P}(n)\,|n\rangle\langle n|\ .\tag{14}$$

Since the number states $|n\rangle$ have zero expectation value for the electric field, here also we find $\left\langle \hat{E}_x \right\rangle_{\text{thermal}} = 0$.

2.2 Experimental setup

We create a setup which allows us to conveniently create coherent and thermal states at will.

We start from a laser: the light it produces is coherent, and thus obeys Poisson statistics. We bounce this laser off a disk, which is covered in sandpaper. The shape of the apparatus is quite simple; it is shown in figure 4. The sandpaper is reflective, so as long as the disk is stationary we expect the statistics of the light to be preserved. We will see that this is experimentally verified.
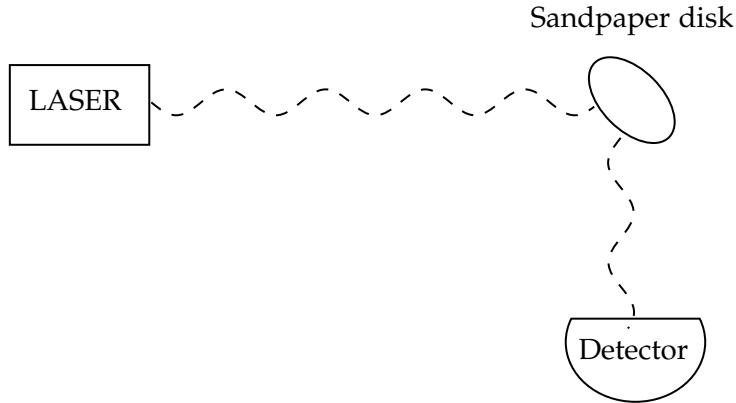

Figure 4: Sandpaper setup.

The sandpaper disk is then spun up: because of the roughness, the exact location from which the light bounces off changes moment by moment, so the electric field is *scrambled*: it loses coherence, and its expectation value over a sufficient period of time becomes zero, which as we saw is a characteristic of thermal light.

2.3 Data preparation

We have two data acquisitions, labelled based on the distribution we expect from them: "coherent" and "thermal". The former is taken with the disk being kept stationary, the latter is taken with the moving disk.

The data from the timetagger is a series of arrival times, in units of its resolution, which is of 80.955 ps.

In order to recover the statistics for a certain acquisition, we select a window size w; divide the total acquisition time into intervals of size w, and count how many photons were detected in each interval.

We then make a histogram of these numbers: after normalization, this procedure yields a probability distribution $\mathbb{P}_w(n)$.

2.4 Analysis

The first kind of analysis one can do is to fit the corresponding distribution to the data. What should we assign as a window size?
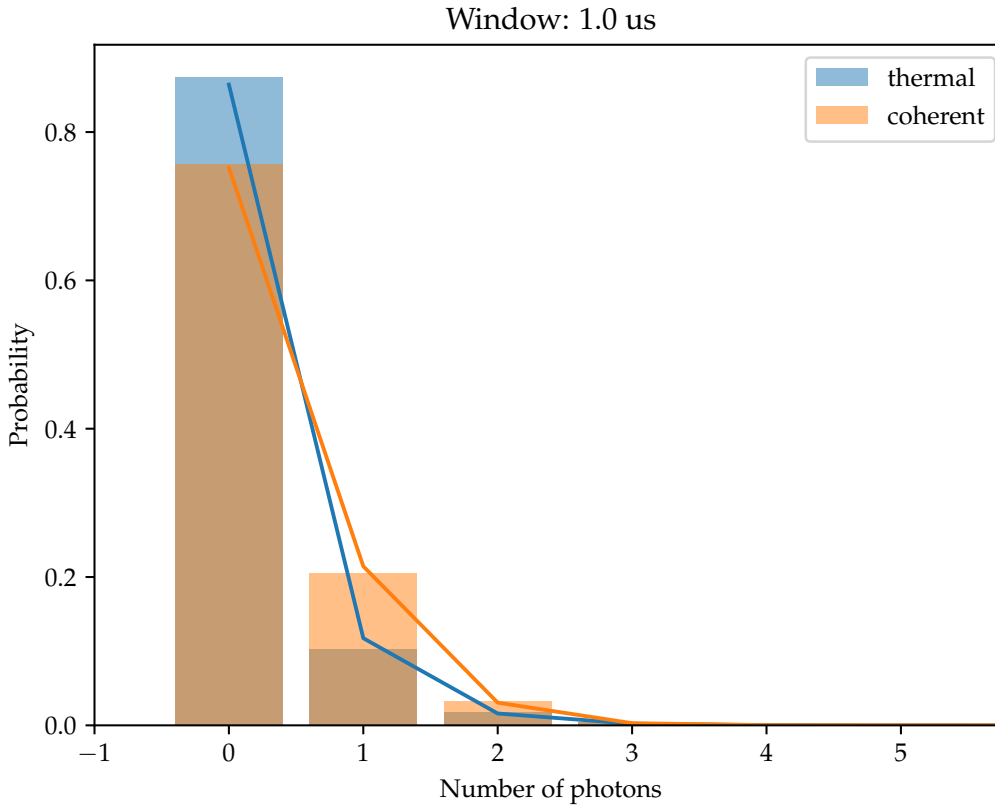

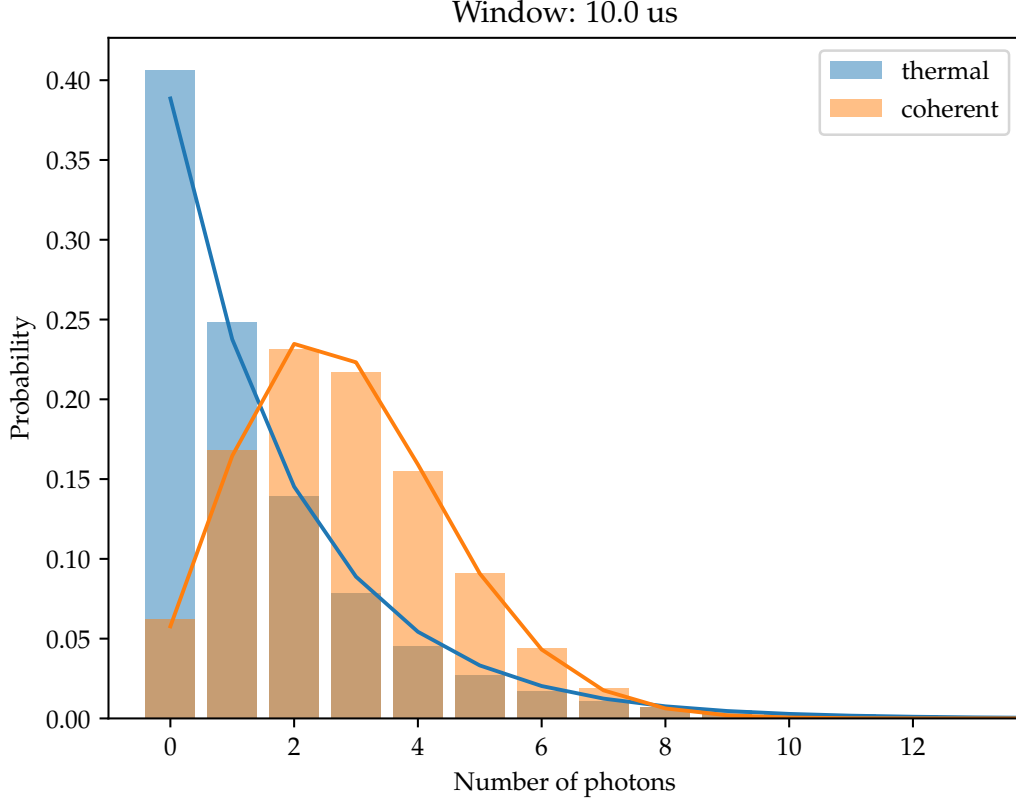Figure 5: Probability of seeing a certain number of photons per window of 1 μs.

Figure 6: Probability of seeing a certain number of photons per window of $10\,\mu s$.

In figures 5, 6 and 7 we show the plots we find with a few different window size possibilities. The histogram is from the data, the line comes from the theoretical distribution computed by fixing the mean to be equal to that of the data.

We can see that with window sizes of the order of $10\,\mu s$ the distribution is close to the theoretical one and the coherent and thermal ones look quite different; for smaller windows we start to rarely see even a single photon per window, for larger ones the mode of the "thermal" distribution shifts from zero.

In order to understand this behaviour more specifically, we can compare the first moments of the distributions to the theoretical ones: we can compute the mean

$$\overline{n} = \sum_n \mathbb{P}(n)n \,, \tag{15}$$

the variance

$$\sigma^2 = \sum_n \mathbb{P}(n)(n - \overline{n})^2 \,, \tag{16}$$

the normalized skewness

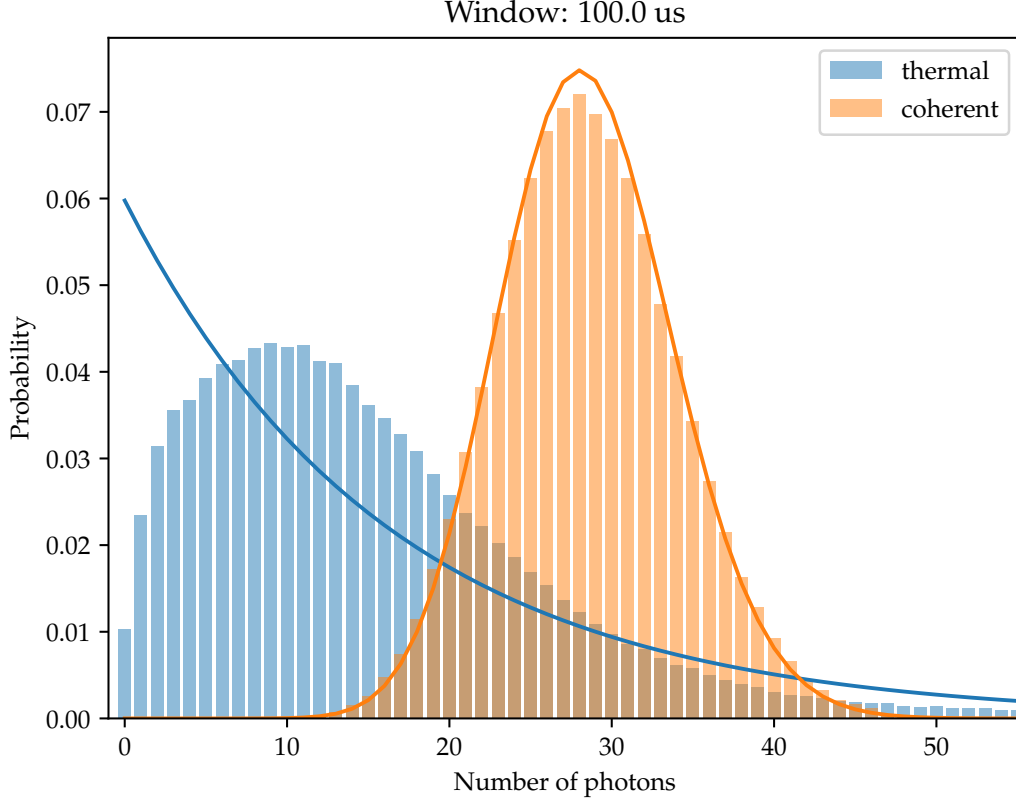$$\text{skewness} = \frac{1}{\sigma^3} \sum_n \mathbb{P}(n)(n - \overline{n})^3 \,, \tag{17}$$

9

Figure 7: Probability of seeing a certain number of photons per window of $100\,\mu s$.

and the normalized kurtosis

$$\text{kurtosis} = \frac{1}{\sigma^4} \sum_n \mathbb{P}(n)(n - \bar{n})^4. \tag{18}$$

For each window size w we compute the moments of the experimental distribution, and the corresponding ones for the theoretical distribution computed by fixing the mean to be the experimental one. The results, for window sizes varying from $10\,ns$ to approximately $3\,ms$, are shown in figure 8. Beyond the moments, the mode is also shown.

We can see that the results trace quite well with the theoretical ones for the coherent case, especially for window sizes of $100\,\mu s$: this is to be expected, and it gives us a way to estimate the coherence length of the LASER.

This is not the case for the thermal state, but it is not a terrible approximation. At $10\,\mu s$ the mean, variance and mode are good, the skewness and kurtosis are a bit off — these higher moments are more influenced by noise at higher photon numbers, so it is understandable that they are more difficult to adjust.

It is understandable that the distribution does not come out to be exactly thermal: what the rotating sandpaper disk does is to effectively remove any kind of phase coherence, and

therefore to enforce the expectation value of the electric field to be zero. Any mixture of number states, however, has this property! The incoming state is still coherent, and with this setup some coherence "shines through": perhaps with more than one rotating disk the state might have enough interactions with the environment to thermalize — this has not fully happened in our case.

References

[con19]   Scipy contributors. *Scipy.Stats.Gaussian_kde — SciPy v1.4.1 Reference Guide*. 2019. URL: https://docs.scipy.org/doc/scipy/reference/generated/scipy.stats.gaussian_kde.html#ra3a8695506c7-1 (visited on 05/30/2020) (cit. on p. 5).

[GRA86]   P Grangier, G Roger, and A Aspect. "Experimental Evidence for a Photon Anticorrelation Effect on a Beam Splitter: A New Light on Single-Photon Interferences". In: *Europhysics Letters (EPL)* 1.4 (Feb. 15, 1986), pp. 173–179. ISSN: 0295-5075, 1286-4854. DOI: 10.1209/0295-5075/1/4/004. URL: https://iopscience.iop.org/article/10.1209/0295-5075/1/4/004 (visited on 04/22/2020) (cit. on p. 1).

[ST]   B. E. A. Saleh and M. C. Teich. *Fundamentals of Photonics*. 3rd ed. Wiley (cit. on p. 6).

[Sco15]   David W. Scott. *Multivariate Density Estimation: Theory, Practice, and Visualization*. John Wiley & Sons, 2015 (cit. on p. 5).

[Tho+04]   J. J. Thorn et al. "Observing the Quantum Behavior of Light in an Undergraduate Laboratory". In: *American Journal of Physics* 72.9 (Aug. 13, 2004), pp. 1210–1219. ISSN: 0002-9505. DOI: 10.1119/1.1737397. URL: https://aapt.scitation.org/doi/10.1119/1.1737397 (visited on 03/25/2020) (cit. on p. 1).
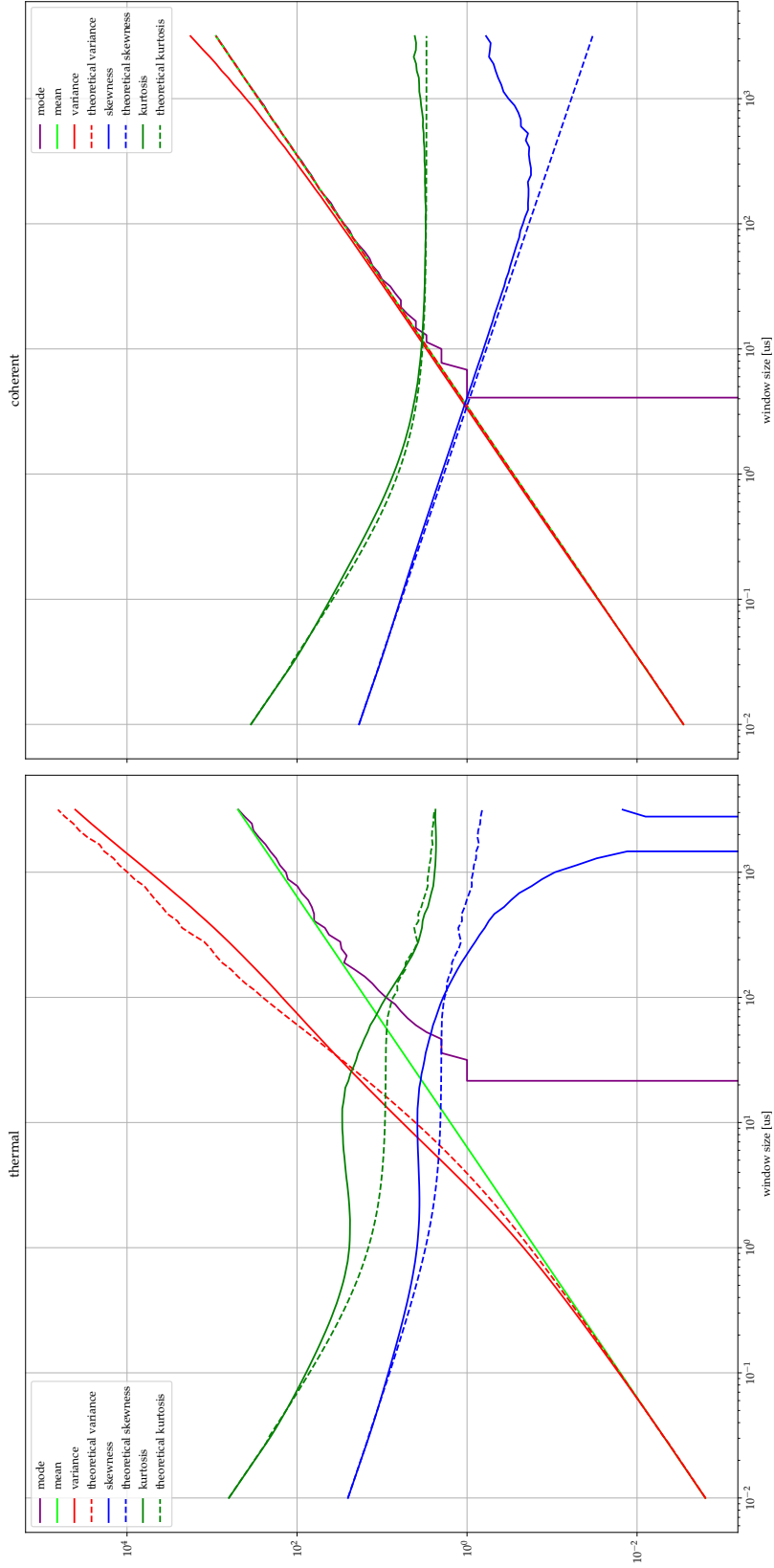
Figure 8: Photon statistics.